Inorganic Chemistry

Article

pubs.acs.org/IC

Electronic Excitations and Lattice Dynamics of Coordinatively "Unsaturated" Complex Transition Metal Compounds

Dana E. Gheorghe,[†,‡] Alexander P. Litvinchuk,[‡,§] and Angela Möller*[,†,‡]

[†]Department of Chemistry, University of Houston, 136 Fleming Building, Houston Texas 77204-5003, United States

[‡]Texas Center for Superconductivity, University of Houston, 2002 Houston Science Centre, Houston, Texas 77204-5002, United States

[§]Department of Physics, University of Houston, 617 Science & Research Building 1, Houston, Texas 77204-5005, United States

ABSTRACT: Single crystal polarized Raman and infrared spectra of the series $Na_5[MO_2][X]$ with M = Co^I, Ni^I, and Cu^I and X = S^{2-} and CO_3^{2-}, are reported. All phonon modes are assigned to the lattice eigenmodes based on the group theory analysis and first principles lattice dynamics calculations. The energies of the fundamental symmetric and asymmetric vibrations of the $[MO_2]^{3-}$ complex are discussed on the basis of their electronic structure and variation in M−O interatomic distances. Electronic Raman scattering and luminescence are observed for the magnetic members of the series (Co^I, d^8, and Ni^I, d^9). Ligand field theory is employed to account for the electronic effects which originate from states split by spin−orbit coupling.

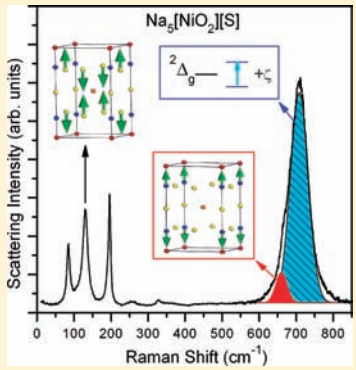

1. INTRODUCTION

Coordinatively "unsaturated" complex transition metal compounds are exceptional because of the unusually low oxidation state of (+1) of the metal ion, as well as the uncommon coordination number two, $[MO_2]^{3-}$, in the solid state. In general, the oxidation state of (+2) or (+3) is typically observed for 3d transition metals with higher oxidation states, for example, $KMnO_4$, frequently found for complex oxides in octahedral or tetrahedral coordination, respectively.[1] Hence, the synthesis of such a distinctive class of compounds brings novel and valuable insights into transition metal oxide chemistry and interesting aspects of the physical properties yet to be investigated. One of the first structurally characterized alkaline metal oxometallate containing the isolated linear complex $[MO_2]^{3-}$ was $K_3[CuO_2]$ reported in 1985 by Hoppe et al.[2] Since then, several other materials have been synthesized by elaborated solid state methods, for example, $K_3[MO_2]$, M = Fe^I, Co^I, Ni^I; $KNa_2[NiO_2]$; $Na_5[MO_2][X]$, M = Co^I, Ni^I, Cu^I and X = CO_3^{2-}, SO_4^{2-}, SO_3^{2-}, S^{2-}.[3−6] Until now the general knowledge of these materials is still limited primarily to their structural aspects. The electronic structures for Ni^+ and Ni^{2+} have been investigated by absorbance spectroscopy and discussed within the framework of the angular-overlap model (AOM).[7−9] Furthermore, for some of these compounds powder infrared data (KBr technique) have been reported with tentative assignments of the antisymmetric stretching vibration of $[MO_2]^{3-}$, which generated some confusion because of the presence of additional carbonate modes in most cases. To the best of our knowledge, complementary Raman data are still missing in spite of the fact that they are crucial for the experimental characterization of all modes of the $[MO_2]^{3-}$ species of the series in the solid state and unraveling their dependence on electronic configuration.

Herein we investigate a series of very moisture sensitive $Na_5[MO_2][X]$ compounds by single crystal Raman and infrared spectroscopy. Our interest in this family of compounds is based on their simple isotypic crystal structures, which allow theoretical work to be successfully carried out. The results of first principle calculations will provide a solid platform for the discussion of structure−property relationships, including aspects of the respective electronic configuration of the transition metal. They will also allow to assign the fundamental vibrations of the $[MO_2]^{3-}$ complex of $Na_5[MO_2][S]$ series. Special attention will be paid to the structural distortions of the framework that renders the fundamental modes of the noncoordinating carbonate hosted in a cube-octahedral cavity of sodium cations. Of the utmost importance are the magnetic species (Ni^+, d^9, and Co^+, d^8) for which the respective electronic structures contribute additional spectral features via electronic Raman scattering and photoluminescence.

2. EXPERIMENTAL SECTION

Synthesis. All starting materials were handled inside an argon filled glovebox (MBraun). The chemicals were commercial grade and used as received: sodium oxide (Alfa Aesar, Na_2O (86−88%), cobalt powder (Alfa Aesar, 99.8%), Cu_2O (Alfa Aesar, 99.9%), nickel powder (Alfa Aesar, 99.8%), CdO (Alfa Aesar, 99.998%), Na_2SO_3 (Alfa Aesar, 98%), Na_2CO_3 (Aldrich, 99.95%), Na_2SO_4 (EMD), and Ag (Oegussa). Crystals of the target compounds were prepared by modified synthesis methods from previously described routes.[5] It was found that large

Received: February 15, 2012
Published: May 3, 2012

   dx.doi.org/10.1021/ic300348b | *Inorg. Chem.* 2012, 51, 5822−5830

excess of Na_2O and Na_2CO_3 provided good quality single crystals of suitable size (e.g., ≈ 0.12 × 0.12 × 0.1 mm) for spectroscopic characterization. The synthetic approaches involved the use of binary compounds, Cu_2O for all cuprates[5] as starting materials whereas for M = Co, Ni the CdO route[10] was applied. All reactions were carried out under an inert gas atmosphere (Ar) in sealed Ag containers which were encapsulated in silica glass ampules. The CdO route involves a redox reaction to achieve the extraordinary low and rare oxidation state of the transition metals and yields metallic cadmium as a side product, which at the annealing temperature acts as a flux enhancing thus the crystallinity of the target compound. The following compounds were synthesized by the CdO route and nonstoichiometric ratios were employed to grow single crystals for the spectroscopic investigations. **$Na_5[CoO_2][CO_3]$** (**1**). Ruby red crystals were obtained typically using 518.3 mg of Na_2O, 244 mg of CdO, 224 mg of Co powder, and 200 mg of Na_2CO_3 in a molar ratio of 4:1:2:1 as starting materials. The reaction was kept at 500 °C for 10 days, and then cooled to room temperature with a rate of 60 °C/d. **$Na_5[NiO_2][CO_3]$** (**2**). Red crystals were prepared using Na_2O, CdO, Ni powder, and Na_2CO_3 as starting materials. Two different ratios and temperature schemes were used, 4:1:2:1 (10 d at 500 °C, cooling rate of 60 °C/d to room temperature) and 2.5:1:2:3, respectively (5 d at 600 °C, cooling rate of 100 °C/d). The later ratio involving 288 mg of Na_2O, 240 mg of CdO, 220 mg of Ni powder, and 570 mg of Na_2CO_3 delivered larger and better crystallized single crystals of compound (**2**). **$Na_5[NiO_2][S]$** (**4**). Red crystals of $Na_5[NiO_2][S]$ were prepared using 185 mg of Na_2O, 113 mg of CdO, 103 mg of Ni powder, and 222 mg of Na_2SO_3 (molar ratio of 3:1:2:2). The mixture was annealed at 600 °C for 10 days and then slowly cooled to room temperature within 4 days. This reaction includes furthermore a disproportion of Na_2SO_3 yielding Na_2S and Na_2SO_4 as intermediates above 500 °C. It should also be noted that compound (**4**) can also be prepared by using Na_2SO_4 instead of Na_2SO_3 at 600 °C and indicates that Ni metal is oxidized by sulfate as well. Since Cu_2O is well-known, we prepared **$Na_5[CuO_2][CO_3]$** (**3**) as yellow crystals from the polynary oxides directly. Typical reactions were carried out using 289 mg of Na_2O, 202 mg of Cu_2O, and 300 mg of Na_2CO_3 in a molar ratio of 3:1:2. The mixture was annealed at 600 °C for 5 days and then cooled to 100 °C with 100 °C/d.

Crystal Structure and Phase Determination. The crystal structures have been reported.[5] Here we used single crystal X-ray diffraction techniques to confirm the phase purity of the target compounds which are very sensitive to moisture. Since decomposition occurs in ambient atmosphere, the selection of suitable crystals for data collection affords sealing in glass capillaries (0.3 mm interior diameter, Charles Supper Company). Single crystal data collection was performed on an APEX II CCD Detector Bruker AXS instrument at room temperature. Lattice parameters were obtained from three sets of frames using the program SAINT (V-7.60A, Bruker). The orientation of selected crystals was determined using a Rapid II (Rigaku) instrument.

Physical Properties. Compounds (**1**–**4**) have been studied by spectroscopic methods, namely, IR and Raman spectroscopy. MIR data were collected in reflectance mode in inert atmosphere on selected single crystals of (**1**–**4**) using an Alpha-P (Bruker Optik) spectrometer (spectral resolution 4 cm^{-1}) build into a glovebox (MBraun). Raman scattering spectra of single crystals of (**1**–**4**) were measured in the backscattering geometry at room temperature on a Horiba Jobin Yvon T 64000 spectrometer equipped with an optical microscope and a liquid nitrogen cooled CCD detector. The spectral resolution did not exceed 2.0 cm^{-1}. We used an Ar^+ laser (λ = 514.5 nm, 2.41 eV), He–Ne laser (λ = 632.8 nm, 1.96 eV) and a near-infrared semiconductor laser (λ = 784.3 nm, 1.58 eV) for excitation. The incident laser power was kept below 1.0 mW to minimize heating of the sample. The diameter of the laser spot was about 2 μm.

Theoretical Work. The first principles density functional calculations of the electronic ground state of the compounds $Na_5[MO_2][S]$ with M = Co^I, Ni^I, Cu^I, were performed within the local density approximation with the Perdew–Wang local functional,[11] using the Dmol^3 code,[12,13] as implemented in the Material Studio package. The integration over the Brillouin zone was performed over the 5 × 5 × 3 Monkhorst-Pack grid in the reciprocal space.[14] The finite displacement method was further used to access the lattice dynamics properties. The ligand field calculations[15] were carried out on the basis of the angular-overlap model (AOM)[9] for the linear $[MO_2]^{3-}$ complexes (M = Co^I and Ni^I) with ligand field parameters (in cm^{-1}) for d^8: B = 780, C = 3200, $(e_\sigma)^{eff.}$ = 5900, e_π = 3000 and for d^9: $(e_\sigma)^{eff.}$ = 6000, e_π = 3000 with $(e_\sigma)^{eff.}$ referring to the effective σ-antibonding interaction including 4s-3d_z mixing, see also refs 6 and 8.

3. RESULTS AND DISCUSSION

Description of the Crystal Structure. The members of the family of $Na_5[MO_2][X]$ are isotypic and crystallize in a tetragonal unit cell depicted in Figure 1. Overall, the structure

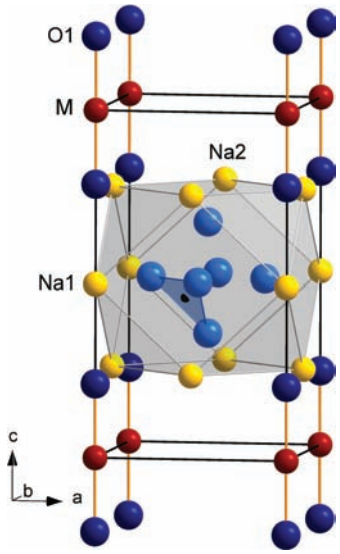

Figure 1. Perspective view of the unit cell of $Na_5[MO_2][CO_3]$, M = Co^I, Ni^I, Cu^I. The carbonate ion is statistically disordered with one out of eight possible orientations indicated (triangle). Note that all oxygen atoms (light-blue) depicted within the cube-octahedral cage are located on crystallographic sites with partial occupancy factors. For $Na_5[MO_2][S]$ only the center (Wyckoff position: 1d) of the cube-octahedral cage is occupied with X = S^{2-}.

can be described as a (double) antiperovskite type of structure according to $\{Na_5M\}_O\{O_2\}_{Ti}\{X,\square\}_{Ca}$ with alternating occupied, X, and empty, □, voids of the formal $\{X,\square\}_{Ca}$ site. The tetragonal unit cell consists of monolayers of transition metal cations (M = Co^I, Ni^I, Cu^I) in a linear "unsaturated" coordination sphere, $[O–M–O]^{3-}$. These layers are separated by sodium cations and noncoordinating anions such as X = CO_3^{2-} or S^{2-}. Slightly distorted cube-octahedral voids formed exclusively by 12 sodium cations incorporate X anions as "guests", whereas those voids, □, formed by 8 sodium and 4 transition metal cations remain empty. It should be noted that the carbonate ion violates the tetragonal symmetry of the unit cell and is consequently statistically disordered. The distortions of the occupied cube-octahedral cages (**1**–**3**) are related to the M–M distances (lattice constant, a) in the range 4.608–4.652 Å. For the X = CO_3^{2-} series a slight elongation of the cube-octahedron along the c axis of 4.62 Å refers to the constant d(Na2–Na2) distances within the standard deviation. For the X = S^{2-} series a compression of the cube-octahedral cage related to d(Na2–Na2) = 3.90 Å is observed. Overall, the c/a ratio of the lattice constants is mainly dictated by the interatomic distance, d(M–O), along [001], and by the size

dx.doi.org/10.1021/ic300348b | Inorg. Chem. 2012, 51, 5822–5830

of X^{2-}, respectively. The former one is depending on the d-orbital splitting for this coordination, with the d_{z^2} and d_{xz}, d_{yz} orbitals at higher energies because of σ- and π- antibonding interactions, respectively, in relation to the essential non-bonding d_{xy} and $d_{x^2-y^2}$ orbitals in an axial ligand field described by the angular-overlap model.[9]

Group Theory Analysis. As the spectroscopic investigations are aimed at studying the vibrational features of the complex ions, $[MO_2]^{3-}$ and $[CO_3]^{2-}$, we will first comment on a group theoretical analysis and discuss our results within the framework of density functional theory (DFT) based analyses for all lattice modes below. Let us first introduce the main features for a "free" carbonate with D_{3h} symmetry for which the following four fundamental modes are expected: totally symmetric stretching, ν_1 (A_1' Raman active), out-of plane deformation, ν_2 (A_2'' IR active), antisymmetric stretching ν_3 (E′), and in-plane bending, ν_4 (E′). Both E′ modes are IR and Raman active.[16−18] As mentioned above, the carbonate ion is statistically disordered in the present structure, therefore, we need to keep in mind the aspect of a possibly lower local symmetry, for example, C_{2v}, originating from the slight elongation of the cube-octahedron effectively distorting the octahedral arrangement of the light-blue marked oxygen atoms (see Figure 1). For simplicity we will refer to the carbonate ion as a "free" ion here and use the D_{3h} symmetry for the assignment of respective modes.

All other ions within this structure type are ordered. Hence, we facilitate our description based on group theory by using $Na_5[MO_2][S]$ to derive the activity of all expected modes in the space group $P4/mmm$ based on the respective fully occupied Wyckoff positions.[5] The irreducible representations[19] give in total 27 phonon modes of which 24 are optical (Γ_{Raman}: $2A_{1g}$ + B_{1g} + $3E_g$; Γ_{IR}: $4A_{2u}$ + $5E_u$; and one silent B_{2u}), and three are acoustic ($\Gamma_{Acoustic}$: A_{2u}+ E_u). If we assume that the $[MO_2]^{3-}$ complex is decoupled from the lattice (Na^+ and S^{2-}), equivalent to a "free" ion, three fundamental modes are expected: ν_s (totally symmetric stretching, A_{1g} Raman active), ν_{as} (antisymmetric stretching, A_{2u} IR active), and δ (bending, E_u IR active). All other Raman and IR active modes are then representing the lattice modes of the framework for the ordered $Na_5[MO_2][S]$ type of structure and will allow us a comparison with observed ones for $Na_5[MO_2][CO_3]$.

$Na_5[MO_2][S]$: Phonon Modes and DFT Results. Figure 2 shows the single crystal Raman spectrum with the assignment of the observed lattice modes for $Na_5[NiO_2][S]$ along with corresponding atomic displacements, as obtained by the DFT calculations. Table 1 summarizes experimental and theoretical data, which are overall in excellent agreement. Only the B_{1g} mode (II) is not observed here for this crystal orientation. We have carried out a Gaussian fit to the very dominant broad peak at 709 cm^{-1} and assign the shoulder at ≈661 cm^{-1} to the A_{1g} (VI) mode, which is well in line with the calculated value of 659 cm^{-1}. It can be seen from the illustration that the A_{1g} (VI) mode is well separated in energy from the other vibrations and involves exclusively the displacement of the oxygen atoms. Therefore, this mode can be regarded as the above-mentioned fundamental symmetric stretching vibration, ν_s, of the $[NiO_2]^{3-}$ unit. The intense line at 709 cm^{-1} is due to electronic Raman scattering and we will comment on this below.

For comparison purposes, we have also carried out DFT calculations for the d^{10} system, $Na_5[CuO_2][S]$, and the results are shown in Table 1. It is worth noting that the DFT calculations indicate the band gap is well above 2.0 eV in agreement with the transparent yellow color of the crystals $Na_5[CuO_2][X]$ with X = S^{2-} and CO_3^{2-}. Hence, no electronic Raman scattering involving electronic states (d-d transitions) is anticipated for experiments using laser excitations of λ = 784.3

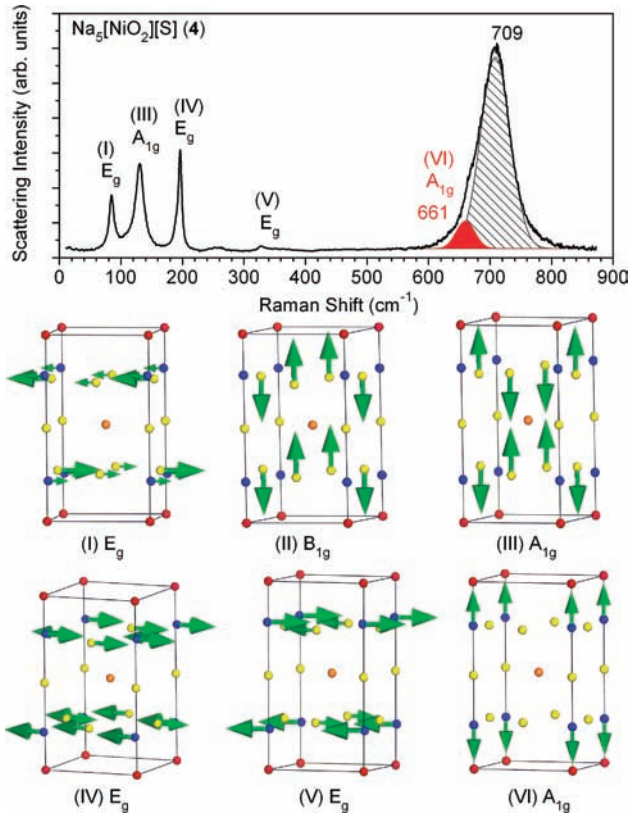

Figure 2. *Top*: Raman spectrum of $Na_5[NiO_2][S]$ (**4**) at $\lambda_{exc.}$ = 632.8 nm. Indicated are the 5 observed modes and the broad intense feature resulting from electronic Raman scattering (gray shaded area). *Below*: Displacement patterns and symmetry of all 6 Raman active lattice vibrations for $Na_5[NiO_2][S]$ as calculated from DFT. (Ni, red; O, blue; Na, yellow; S, orange).

Table 1. Comparison of DFT Calculated Vibrational Modes with Experimental Data for $Na_5[MO_2][S]$[a]

M=Cu calc.	M=Co calc.	M=Ni calc.	M=Ni exp.	$Na_5[MO_2][S]$ assignment
88	91	83	85	E_g (I)
91	*99*	*83*		E_u
116	112	105		B_{1g} (II)
139	137	111	≈132	A_{1g} (III)
130	*138*	*118*		E_u
138	*158*	*140*		E_u
171	*177*	*158*		A_{2u}
179	*196*	*171*		A_{2u}
192	*197*	*182*		A_{2u}
199	191	194	196	E_g (IV)
231	*235*	*229*		$E_u^{(1)}$
255	*313*	*254*		A_{2u}
324	422	315	329	E_g (V)
346	*432*	*337*		$E_u^{(2)}$
622	703	659	661	A_{1g} (VI) [ν_s]
641	*737*	*685*	*695*	$A_{2u}^{(3)}$ [ν_{as}]

[a]The assignment for Raman active and infrared active (*italic*) modes include the labels in brackets referring to the representations given in Figure 2.

dx.doi.org/10.1021/ic300348b | *Inorg. Chem.* 2012, 51, 5822−5830

or 632.8 nm in contrast to (**1**, **2**, **4**), see below. Figure 3 shows polarized single-crystal Raman spectra recorded for $Na_5[CuO_2][CO_3]$ in comparison with a powder spectrum of γ-Na_2CO_3.

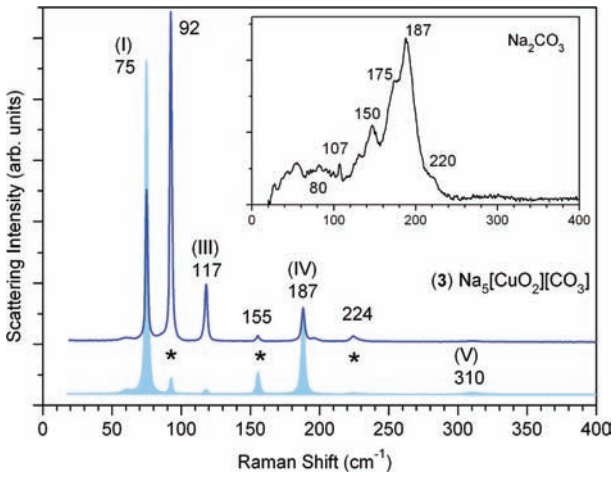

Figure 3. *Main panel:* Low-energy part of the Raman spectra of $Na_5[CuO_2][CO_3]$ (**3**) for crossed (lower cyan, filled) and parallel (upper blue line) polarizations of the incident scattered light with assignments (I–V) based in Table 1 and $Na-O^{carbonate}$ lattice modes (*). *Inset*: Powder spectrum ($\lambda_{exc.}$ = 784.3 nm, T = 300 K) of γ-Na_2CO_3.

First, let us compare the DFT results of $Na_5[MO_2][S]$ series. Overall, we note that the calculations predict rather similar lattice modes, except for those associated with the $[MO_2]^{3-}$ units. The A_{1g} (VI) mode, ν_s, of the $[CuO_2]^{3-}$ unit, for example, is calculated at the lowest energy, 622 cm^{-1}, as expected for longer interatomic d(Cu–O) distances by about 0.03 Å if compared with d(Ni–O) or 0.04 Å for d(Co–O). We observe ν_s at ≈620 cm^{-1} for $Na_5[CuO_2][CO_3]$ (Figure 4). The consistency of this assignment is further corroborated by recent Raman experiments reporting ν_s = 604 cm^{-1} for $K_5[CuO_2][CO_3]$.[20] The trend of higher energy modes for shorter distances is clearly shown for the calculated symmetric and antisymmetric stretching modes of the $[MO_2]^{3-}$ complex, see below. In the case of M = Co the lattice modes that involve bending displacements are shifted remarkably to higher wavenumbers. One reason might be attributed to electronic effects for a d^8 configuration which we will discuss below.

At this point it is important to separate the phonon modes into two categories, the so-called lattice modes of the framework and the ones associated with the complex units, $[MO_2]^{3-}$ and CO_3^{2-}. If we now neglect the modes originating from the X ion contributions for the $Na_5[MO_2][X]$ series, we would anticipate rather similar lattice modes of the ordered Na–M–O framework. Figure 3 indeed shows those modes labeled at 75 (I), 117 (III), 187 (IV), and 310 (V) for $Na_5[CuO_2][CO_3]$, that exhibit only small shifts if compared with $Na_5[NiO_2][S]$. Keeping in mind that all the modes just listed are entirely due to Na–O displacements, the additional phonon modes at 92, 155, and 224 cm^{-1}, marked with an asterisk in Figure 3, are thus linked to $Na-O^{carbonate}$ vibrations of the carbonate occupying statistically the cube-octahedral void of the framework. The inset of Figure 3 shows the powder Na_2CO_3 Raman spectrum for comparison and indicates nicely the principal region of $Na-O^{carbonate}$ lattice modes. Single

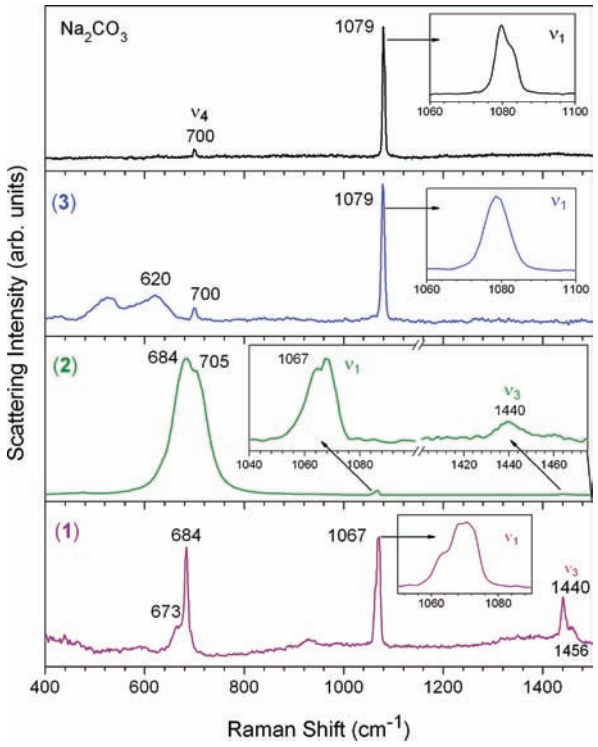

Figure 4. *Main panel*: Powder Raman spectrum of γ-Na_2CO_3 (top, $\lambda_{exc.}$ = 784.3 nm) and single crystal Raman spectra $Na_5[MO_2][CO_3]$ with M = Cu (**3**, blue, $\lambda_{exc.}$ = 632.8 nm), Ni (**2**, green, $\lambda_{exc.}$ = 632.8 nm), and Co (**1**, purple, $\lambda_{exc.}$ = 784.3 nm) at 300 K. *Insets*: Enlargements of all ν_1 assigned fundamental carbonate mode and ν_3 for (**2**).

crystal Raman spectra for $Na_5[MO_2][CO_3]$, M = Co^{I} and Ni^{I}, are given below (Figure 8, 9) showing similar modes in agreement with the calculated ones of the Na–M–O framework in the region below 400 cm^{-1}.

$Na_5[MO_2][CO_3]$: Phonon Modes above 400 cm^{-1}. The Raman and infrared spectra above 400 cm^{-1} of the fundamental modes of the almost "free" $[CO_3]^{2-}$ and $[MO_2]^{3-}$ units are shown in Figures 4 and 5 in comparison with γ-Na_2CO_3 for a reference. It can be seen that (**2**) like (**4**) show nonphonon (electronic) contributions to the Raman scattering, which complicates the assignment of the symmetric stretching ν_s for the $[NiO_2]^{3-}$ units. Therefore, we will first discuss the spectral features of the carbonate present in the cube-octahedral cavity.

As previously mentioned, there are four fundamental modes of the carbonate: ν_1 (A_1' Raman active), ν_2 (A_2'' IR active), ν_3 (E′), and ν_4 (E′), with both E′ modes are IR and Raman active. Overall, we observe the totally symmetric stretching mode of the $[CO_3]^{2-}$ ion, ν_1, as a strong and sharp peak centered around 1070 cm^{-1} (approximate half-width of 10 cm^{-1}, see also insets of Figure 4) for all $Na_5[MO_2][CO_3]$ (**1**–**3**) compounds. It is interesting to note that ν_1 is shifted toward higher wavenumbers for (**3**) if compared with (**1**, **2**). The distortion of the cube-octahedral cavity depends mainly on the respective lattice constants, a_M, for this series of compounds (**1**–**3**), whereas the elongation along the c-axis remains constant within the standard deviation. The lattice constant a_{Cu} is found to be 0.019 Å shorter than a_{Ni} and even 0.044 Å shorter if compared to a_{Co}. This indicates that the cage, in which the carbonate ion is confined in a statistically disordered setting, is large enough for (**1** and **2**) to be close to the "free" ion behavior associated with ν_1 = 1063 cm^{-1}.[21] The hypsochromic shift of ν_1 for (**3**) by

dx.doi.org/10.1021/ic300348b | Inorg. Chem. 2012, 51, 5822–5830

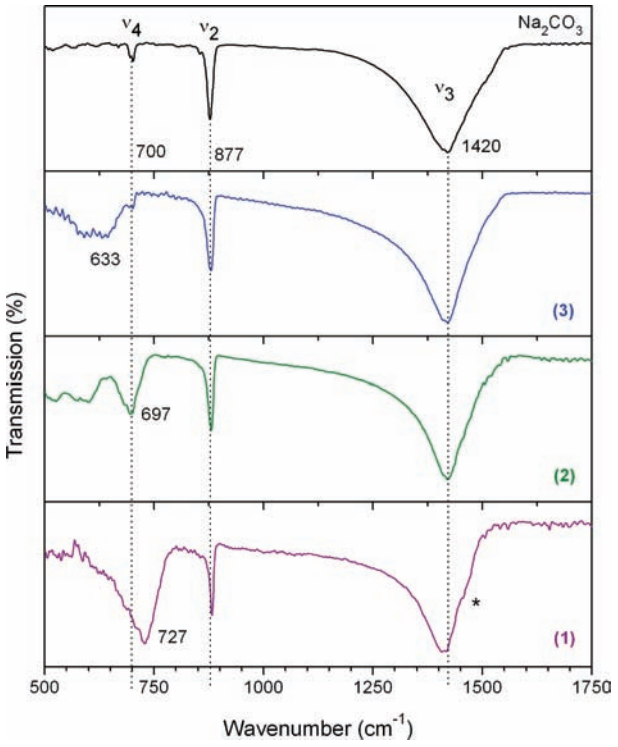

Figure 5. Comparison of the IR spectra of γ-Na_2CO_3 (top) and $Na_5[MO_2][CO_3]$ with M = Cu (**3**, blue), Ni (**2**, green), Co (**1**, purple). The dotted lines are guidelines for the IR active fundamental modes of the carbonate ion, ν_4, ν_2, and ν_3 (from left to right) and (*) denotes a weak shoulder present for (**1**).

12 cm^{-1} of the symmetric peak toward 1079 cm^{-1} is, on the other hand, in excellent agreement with the main feature observed for γ-Na_2CO_3 at the same energy, but asymmetric for the latter one, clearly exhibiting a shoulder at 1083 cm^{-1} (reported: 1080 and a shoulder at 1085 cm^{-1}, respectively).[17,22,23] For the compounds (**1** and **2**) a shoulder at lower energies is observed, clearly indicating at least two slightly different carbonate ions being present, since ν_1 is a nondegenerate mode (A_1').

The second nondegenerate mode of the carbonate, ν_2, is only infrared active and can be observed at 877 cm^{-1} for γ-Na_2CO_3 and at 880 cm^{-1} for all compounds (**1**–**3**), as shown in Figure 5. The antisymmetric stretching, ν_3 (E′), is observed in the IR at 1420 cm^{-1} (broad) which is very close to the reported one of 1415 cm^{-1}.[22,23] In the case of (**1**) a weak shoulder at higher energies (≈ 1445 cm^{-1}) is noticeable in the infrared spectrum. For γ-Na_2CO_3 and (**3**) we do not observe this mode in the Raman experiment, but a sharp feature with a shoulder occurs for (**1** and **2**) at 1440/1456 cm^{-1}. The question arises as to why does ν_3 appear at higher wavenumbers in the Raman spectra in comparison to the IR spectra? Let us first consider what would lift the degeneracy of E′. One reason may be attributed to a lower local symmetry of the carbonate ion, for example, C_{2v}; in this case the nondegenerate modes $A_1 + B_1$ should be both infrared and Raman active, but it would not explain the significant shift of more than 20 cm^{-1} for ν_3. Another scenario of inducing a splitting and a significant shift in particular to ν_3 includes the effect of the crystal field, which may cause the perturbed crystalline modes to be observable in either Raman or IR spectra.[21] In fact these authors, as well as Brooker and Bates,[23] found that the difference between the IR and the Raman modes can even exceed $\Delta_{(R\text{-}IR)} \approx 20$ cm^{-1} for ν_3 and reported Raman shifts of 1448 cm^{-1}. It remains unclear at this point whether excitation into electronic states as observed for (**1**, **2**) plays a significant role to account for this shift in energy as well. In principle, substantial distortion is imposed on the Na–O framework originating from an excited state of the respective transition metal, elongation of d(M–O) results, and thereby effectively altering the size of the cavity in which the carbonate is confined.

The second E′ mode, the in-plane bending, ν_4, has caused the major ambiguity in assigning the ν_s and ν_{as} of the $[MO_2]^{3-}$ unit correctly thus far, because all three are very close in energy. Here we observe a comparably weak ν_4 peak of the carbonate at 700 cm^{-1} for γ-Na_2CO_3 and (**3**) in the infrared spectra and note that it is obscured by broader lines at 697 cm^{-1} (**2**) and 727 cm^{-1} (**1**), as shown in Figure 5. Thus, we assign the broad feature at ≈633 cm^{-1} (**3**) to ν_{as}^{Cu}, in good agreement with the DFT calculations. Moreover, our assignment of ν_{as}^{Ni} = 697 cm^{-1} (**2**) is also supported by the observation of a similar strong peak in the infrared spectrum of (**4**), see also Table 1. The comparatively shorter interatomic distance d(Co–O) is in accord with the assignment of the line at 727 cm^{-1} to ν_{as}^{Co} and in excellent agreement with the overall trend resulting from our lattice dynamics calculations. As far as the Raman spectra in the range of interest are concerned, the ν_4 vibration occurs at the same energy (700 cm^{-1}) and with a similarly weak relative intensity compared to ν_1 for γ-Na_2CO_3 and (**3**). A weaker and sharper feature (684 cm^{-1}) is overlapping with the intense electronic Raman scattering band for (**2**) and is carrying both phonon contributions of ν_s^{Ni} and ν_4. This feature will be discussed in mode details further. For (**1**) a sharp peak, similar in intensity to ν_1, is observed at 684 cm^{-1} and seems to be superimposed on a broader feature at about 673 cm^{-1}, presumably representing the ν_s^{Co} mode (Figure 4). This assignment is in line with the shorter interatomic distance M–O for M = Co^{I} in comparison with M = Cu^{I} and Ni^{I}, see also Figure 6 for a comparison. Moreover, the assignment of ν_4 to ≈684 cm^{-1} (**1**, **2**) and 700 cm^{-1} (**3**) is in reasonable agreement with the reported "free" ion value of 680 cm^{-1}.[24]

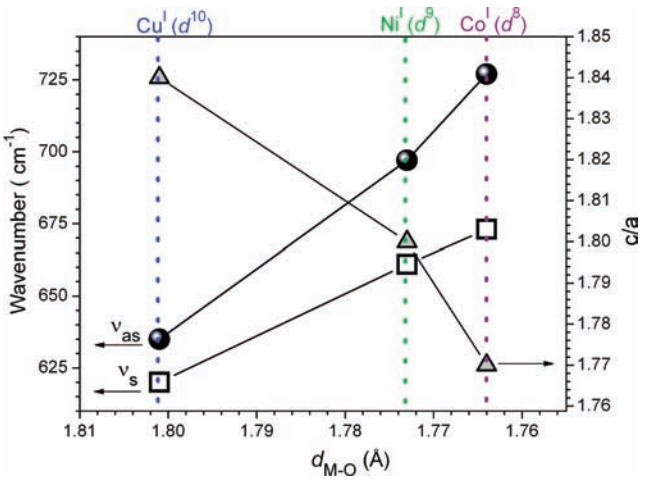

Figure 6. Interatomic distances d(M–O) versus the c/a ratio of the lattice parameters (triangles) and the stretching mode frequencies, ν_{as} (circles) and ν_s (squares), of the $[MO_2]^{3-}$ complex in $Na_5[MO_2][CO_3]$ with M = Cu (**3**, blue), Ni (**2**, green), Co (**1**, purple). The solid arrows and colored dotted lines are guidelines for the eye.

dx.doi.org/10.1021/ic300348b | *Inorg. Chem.* 2012, 51, 5822–5830

It is worth noting several aspects, which are striking in the case of (**1**, **2**): First, is a pronounced intensity increase of ν_4 related to electronic Raman scattering? Second, in both cases the ν_4 modes are found red-shifted by 16 cm^{-1} in a similar way as ν_1 (see above: strain/size effect by the cavity). Third, the peak assigned to ν_1 is asymmetric. Fourth, only in these cases ν_3 shows significant intensity in the Raman spectra.

$[MO_2]^{3-}$: Phonon Modes and Electronic Structure. Keeping in mind that ν_4, ν_s, and ν_{as} are of similar energies around 700 cm^{-1}, we evaluate our observations by exploring the interatomic distances d(M−O) versus c/a ratio of the lattice parameters (Figure 6). First, we note that the interatomic distances d(M−O) elongate considerably from a d^8 to a d^{10} electronic configuration, with additional electrons occupying the π^* (d^9) and σ^* (d^{10}) orbital sets, respectively. The ligand field splitting for the C.N. 2 in the case of a π-donor such as O^{2-} follows the sequence in energy: $d_{z^2} > d_{xz}$, $d_{yz} > d_{xy}$, $d_{x^2-y^2}$. Therefore, the overall trend of the relation between the interatomic distance and the electronic structure of an isolated complex can be well understood within this simple picture. Furthermore, in general σ^* interactions are much stronger effecting the elongation of a bond than π^* interactions (see also ref 6 and 8 for further details). The overall trend in increasing the M−O distances is well represented by the bathochromic shift of the stretching vibrations, ν_s and ν_{as}. Both modes are close in energy for each structure. This is rather unexpected and may have led to some confusion in earlier experimental and theoretical reports on the isolated $[MO_2]^{3-}$ complex. The present spectroscopic study on single crystals, that encompasses most members of the series, allows us to unambiguously conclude that in fact ν_{as} is only slightly higher (≈20−50 cm^{-1}) in energy than ν_s. Our DFT calculations of the $Na_5[MO_2][S]$ compounds are in excellent agreement with the ν_{as} modes observed for (**1**−**3**) and for ν_s (**2**,**3**), respectively. Only the ν_s^{Co} (**1**) is found at significantly lower energies (Δ = 30 cm^{-1}). As we will discuss below, softening of this mode might be attributed to a possible slight bending originating from the peculiar ligand field splitting for a d^8 configuration here.

It has been suggested that the third mode for a $[MO_2]^{3-}$ complex (δ) could be helpful to resolve the issue of assigning the stretching vibrations of the $[MO_2]^{3-}$ complex within the series. Reported calculations for the $[NiO_2]^{3-}$ complex based on local density-functional (LDF) theory using three types of models, namely, Vosko−Wilk−Nusair local spin-density (LSD) approximation (VWN), the Becke nonlocal functional for exchange (BP), and the Perdew nonlocal functional for correlation (MIX), assign δ as 156 cm^{-1} (VWN), 206 cm^{-1} (BP), and 189 cm^{-1} (MIX), respectively.[25] Our DFT calculations for $Na_5[MO_2][S]$ clearly show that there are two lattice modes associated with the bending of the $[MO_2]^{3-}$ complex, $E_u^{(1)}$ = 229 cm^{-1} and $E_u^{(2)}$ = 337 cm^{-1} for M = Ni (see Table 1). For $E_u^{(1)}$ there is a significant contribution from the displacement of the sodium cations along with the oxygen in-(x-y)-plane motion, whereas the higher energy mode $E_u^{(2)}$ originates almost exclusively from oxygen (Figure 7).

For the electronic structure of $Na_5[CoO_2][CO_3]$ (**1**) the orbital degenerate set, d_{xz} and d_{yz}, is occupied by an uneven number of electrons (d^8 configuration). One possibility of lifting the degeneracy of the ground state is bending, which may be directly related to the above-mentioned δ-modes. It is interesting to mention that the $E_u^{(2)}$ mode is shifted significantly to higher wavenumbers if the $[CoO_2]^{3-}$ complex is kept linear in the DFT calculations. We also note that the

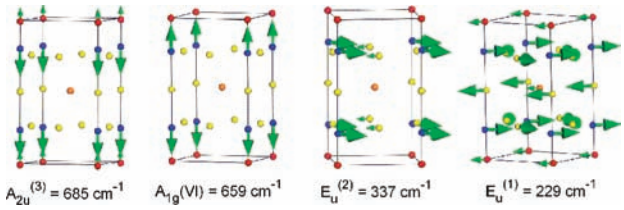

Figure 7. Eigenmodes of the $[MO_2]^{3-}$ complex in $Na_5[NiO_2][S]$ as derived from DTF calculations.

(electronic) effect leading to a bent complex could possibly be responsible for our difficulties in performing the DFT calculations for $Na_5[CoO_2][S]$. Consequently, the true local symmetry of the $[CoO_2]^{3-}$ is then reduced from $D_{\infty h}$ to C_{2v} in this case. At the same time, the proposed bending for $[CoO_2]^{3-}$ might explain the following observations: (i) a significant a lattice constant increase from Ni to Co (see Figure 6), (ii) the higher intensity of ν_{as} relatively to $\nu_2^{(carbonate)}$ = 880 cm^{-1}, see Figure 5, (iii) the broader IR feature at ≈650−700 cm^{-1}, that may carry both modes of ν_{as} and ν_s, as the latter becomes infrared active for C_{2v} symmetry. In Figure 9 (top panel), we tentatively assign a weak feature with a Raman shift of ≈900 cm^{-1} to the $\nu_2^{(carbonate)}$ mode arising from induced distortions of the framework effectively lowering the symmetry of the carbonate in the cavity as well.

$Na_5[NiO_2][X]$: Electronic Raman Scattering. Besides the lattice modes described above, scattering spectra of the $Na_5[NiO_2][X]$ compounds (**2**, **4**) exhibit several additional features. The Raman spectra shown in Figure 2 and Figure 8 (left panel) for laser excitation energies of $\nu_{exc}^{(1)} \approx 12750$ cm^{-1} and $\nu_{exc}^{(2)} \approx 15800$ cm^{-1} reveal the very prominent feature at ≈705 cm^{-1} (*), the intensity of which appears orders of magnitude higher than that of the phonon modes (**2**). This feature, which is also much broader if compared to the lattice modes, is definitely of Raman (and not photoluminescence) origin as its position is "rigidly linked" to the excitation laser line. Indeed, for $\nu_{exc}^{(2)}$ it has the same position (Raman shift) with respect to the laser excitation line, as shown in the left upper panel of Figure 8.

What could be the origin of this line? The right panel of Figure 8 summarizes the results of our electronic structure calculations[15] for a $[NiO_2]^{3-}$ complex within the framework of the angular-overlap model, AOM[9] including spin−orbit coupling (ζ). Two excited levels are derived, $^2\pi_g$ and $^2\Delta_g$, in line with a previous report[7] on the absorbance spectrum of (**2**). Both degenerate excited states are split by spin−orbit coupling ($\zeta \approx 350$ cm^{-1}), whereas the ground state remains an orbital singlet. Hence, the highest excited state $^2\Delta_g \approx 12100$ cm^{-1} splits into two components (12400 and 11680 cm^{-1}, respectively) with the higher one of almost the same energy as the laser excitation $\nu_{exc}^{(1)}$. Therefore, it is reasonable to assume that excitation into the $^2\Delta_g$ will occur as long as the laser energy is in close vicinity to this level, which is actually the case for both excitation energies used here. Further, the Raman scattering process may involve these electronic states as intermediate in the scattering process (see, e.g., ref 26) and thus probe the underlying "electronic structure". Therefore, we believe that the observed intense feature at ≈705 and 709 cm^{-1} in the Raman spectra of (**2**, **4**) can be interpreted as electronic Raman scattering originating from the states of the $^2\Delta_g$ excited multiplet of the $[NiO_2]^{3-}$ complex. Its position is in good

dx.doi.org/10.1021/ic300348b | Inorg. Chem. 2012, 51, 5822−5830

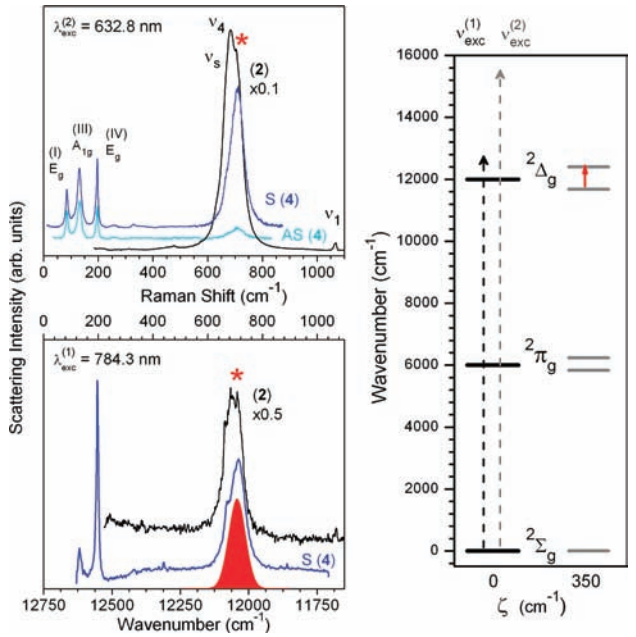

Figure 8. *Left:* Comparison of the Raman spectra of $Na_5[NiO_2][CO_3]$ (**2**) and $Na_5[NiO_2][S]$ (**4**) recorded at laser wavelengths $\lambda_{exc}^{(1)}$ = 784.3 nm (below) and $\lambda_{exc}^{(2)}$ = 632.8 nm (above). Fundamental phonon modes are referenced and the marked feature (*, red, offset: Gaussian fit below) indicates electronic Raman scattering. Raman shifts for (**4**) are shown as S (Stokes) and AS (Anti-Stokes, inverted energy scale) spectra. *Right:* Ligand field splitting in the absence (black) and presence (gray) of the spin–orbit coupling, ζ. The assigned electronic states refer to the $[NiO_2]^{3-}$ complex for $D_{\infty h}$ symmetry. The red vertical arrow indicates the electronic Raman scattering transition, and dashed lines show the excitation quanta.

agreement with the calculated difference in energy (720 cm^{-1}) of the two levels arising from spin–orbit coupling.

Even though it appears unusual to observe the electronic Raman scattering processes involving an excited multiplet, we stress that the ground state is an orbital singlet and, correspondingly, any intermultiplet electronic transitions are absent. Of course, the population of high-lying excited states is expected to be extremely low at room temperature. On the other hand, because of the isolated nature of $[MO_2]^{3-}$ complexes one could expect an enhanced lifetime. This and the population increase by application of up to 1 mW laser power on a 1 μm^2 area of a single crystal turns out to be sufficient to allow the experimental observation of an electronic transition within a higher excited state. Despite of the fact that we did not perform a systematic study of relative intensities of lines in the Raman spectra as a function of power of laser radiation, we did observe an increase of the intensity of the "electronic peak" with respect to phonon lattice modes upon increase of the incident laser power. This fact implies a superlinear intensity dependence of the former electronic feature and, again, points toward its non-phonon origin.

For (**4**) the Stokes and anti-Stokes Raman spectra are compared for $\nu_{exc}^{(2)}$ and clearly show the expected difference in intensity for the electronic Raman scattering, which depends on the population of the excited electronic states. As a result, the electronic Raman scattering around 709 cm^{-1} renders low for the anti-Stokes spectrum. We also note the broadening to lower wavenumbers in here that can be attributed to the phonon mode ν_s^{Ni} = 661 cm^{-1}. For the other spectra of (**2**, **4**), its signature reveals itself as a shoulder of the dominant electronic feature, see also the band convolution (Gaussian fit) above. Note that the sharper feature at 684 cm^{-1} (**2**) carries the ν_4 carbonate mode.

$Na_5[CoO_2][CO_3]$: Luminescence. In contrast to $Na_5[CuO_2][CO_3]$ (**3**) and $Na_5[NiO_2][S]$ (**4**) where sharp lattice modes in the Raman spectra below 400 cm^{-1} (see also above) can be observed, we find for (**1**) much broader and intense features between 200 and 350 cm^{-1}. If we take into consideration that the ground states for a d^9 (**2**, **4**) and a d^8 (**1**) system differ in terms of their splitting because of spin–orbit coupling (see the panels in Figures 8 and 9 on the right), it may explain the observation of additional electronic features for (**1**). All triplet states of (**1**) are subject to spin–orbit coupling and the calculated splitting of the $^3\pi_g$(F) state gives the energies at ≈355, 235, 118 cm^{-1} above the ground level. Laser excitation energies of $\nu_{exc}^{(1)}$ ≈ 12750 cm^{-1}, $\nu_{exc}^{(2)}$ ≈15800 cm^{-1}, and $\nu_{exc}^{(3)}$ ≈ 19450 cm^{-1} have been used to resolve the difficult assessment of electronic Raman scattering and luminescence in (**1**). The right panels of Figure 9 suggest that excitation into electronic states may occur to a number of excited states. More precisely, $\nu_{exc}^{(1)}$ and $\nu_{exc}^{(3)}$ are close to spin-forbidden excited states (singlets), whereas $\nu_{exc}^{(2)}$ may lead directly to a resonant excitation into the degenerate spin-allowed $^3\pi_g$(P) state.

First, we will focus on the Raman spectra of $Na_5[CoO_2][CO_3]$ (**1**), as shown in the top left panel of Figure 9. The fundamental phonon modes of the carbonate as well as ν_s^{Co} are labeled for $\nu_{exc}^{(1)}$ and have been discussed in detail above. The phonon modes associated with the framework appear at lower wavenumbers and despite their enhanced broadness, if compared with (**2**) or (**3**), may be tentatively assigned based on our previous analysis to E_g(I) ≈ 90, A_{1g}(III) ≈ 140, E_g(IV) ≈ 190, E_g(V) ≈ 400 cm^{-1}, respectively, with the additional $Na-O^{carbonate}$ modes around 105, 155, 175, and 215 cm^{-1}. Note here, that we have chosen E_g(V) ≈ 400 cm^{-1} in accordance with the DFT calculations, but an assignment to 310 cm^{-1} resembling (**3** and **4**) might as well be in principle feasible. The reason for our choice is based on the occurrence of the two very prominent features at ≈260 and 320 cm^{-1} which clearly remain visible while changing the excitation energy to $\nu_{exc}^{(2)}$ and $\nu_{exc}^{(3)}$ and therefore should be of a different origin. All other phonon modes, in particular those of the host lattice, decrease significantly in intensity and almost vanish at $\nu_{exc}^{(3)}$. On passing, recall that the tentatively assigned ν_2 mode and ν_3 are both infrared active for D_{3h} symmetry, but will gain intensity in the Raman upon distortion. Along this line it is conceivable that an excitation of Co^+ into an electronic state leads to an elongation of the Co–O distances which can be accounted for an additional distortion of the framework. Note that ν_s^{Co} is observed for all excitation energies. Overall, the intensity and broadness of the features in the region below 450 cm^{-1} suggest some electronic contribution if compared with the sharp phonon modes at higher energies.

The excitation energy $\nu_{exc}^{(1)}$ is close to a singlet state at 12100 cm^{-1} (see the right panel of Figure 9). Hence, additional electronic Raman scattering below 400 cm^{-1}, associated with the spin–orbit splitting levels of the ground state, might result. In fact, the two features that are observed at ≈260 and 320 cm^{-1} are in reasonable agreement with the calculated splitting of 235 and 355 cm^{-1} for the $^3\pi_g$(F) ground state. The same arguments might be used for the excitation energy of $\nu_{exc}^{(3)}$ into a spin-forbidden excited singlet state at 19230 cm^{-1} resulting likewise in Raman scattering featuring the orbital-splitting of

dx.doi.org/10.1021/ic300348b | *Inorg. Chem.* 2012, 51, 5822–5830

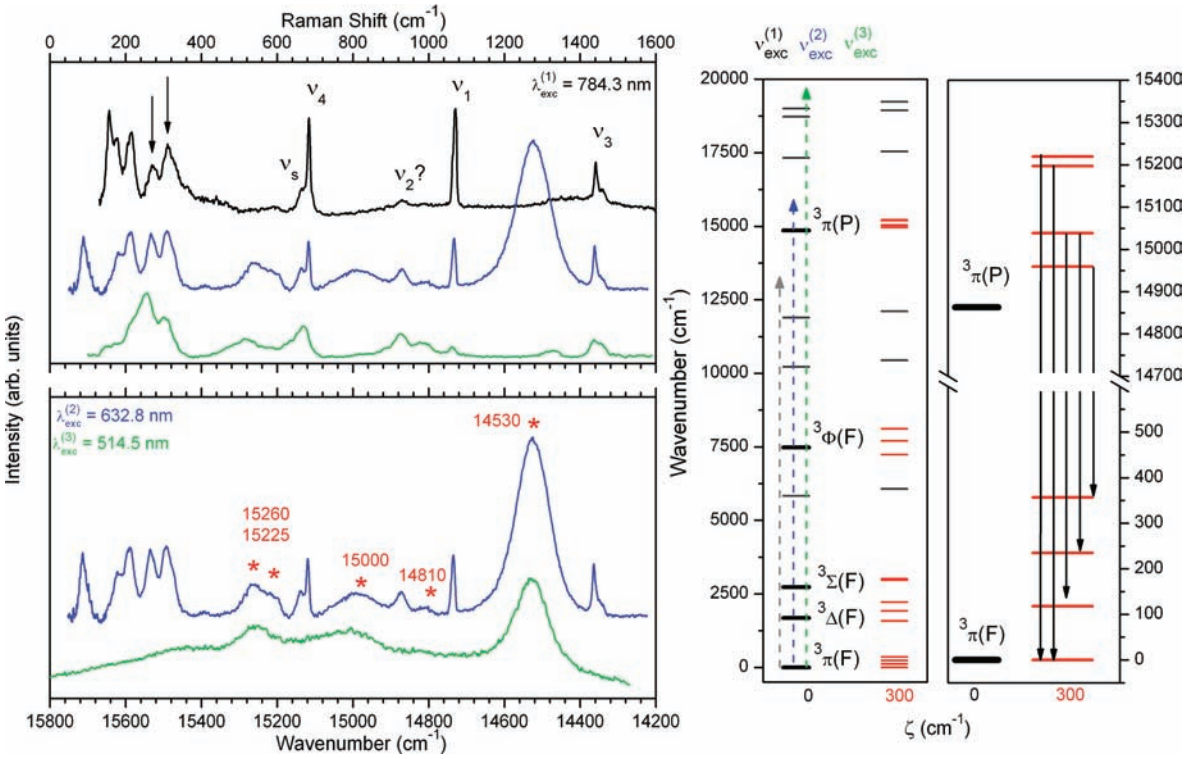

Figure 9. *Left:* The top panel summarizes the Raman spectra of $Na_5[CoO_2][CO_3]$ recorded at λ_{exc} = 784.3 nm, 632.8 nm, and 514.5 nm laser wavelengths, and fundamental phonon modes are referenced. The bottom panel shows the spectra of secondary radiation in the range 14200−15800 cm^{-1}, with the Raman shift with respect to 632.8 nm laser line shown on the top. The (*) asterisk symbols indicate the calculated position of luminescence transitions. *Right:* Ligand field splitting in the absence (black) and presence (red) of spin−orbit coupling, ζ. Only the spin-allowed triplet states of the $[CoO_2]^{3-}$ complex for $D_{\infty h}$ symmetry are assigned here. Dashed lines are used as a guideline to the eye.

the ground state at the same wavenumbers as for $\nu_{exc}^{(1)}$ and $\nu_{exc}^{(2)}$.

For the excitation quanta $\nu_{exc}^{(2)}$, which resonantly excite the $^3\pi_g(P)$ state, several additional levels become important, and optical transitions with calculated energies of 15220, 15200, 15040, and 14960 cm^{-1}, could be realized. The bottom panel of Figure 9 shows the spectra in the relevant energy interval and clearly reveals the marked additional features as luminescence occurring from these spin−orbit levels of the $^3\pi_g(P)$ state into the split levels of the ground state, $^3\pi_g(F)$. The five possible transitions (*) are depicted in the panel on the right by black arrows and are in very good agreement with our ligand field calculations. Experimentally, the three pronounced bands (15260, 15000, and 14530 cm^{-1}) do appear in the luminescence spectrum for $\nu_{exc}^{(3)}$. However, all luminescence features are missing in the spectra under $\nu_{exc}^{(1)}$ as the excitation quanta do not populate the excited $^3\pi_g(P)$ state.

An open question remains regarding the nature of the features at 530 and 990 cm^{-1} in the Raman shift spectra. One possible explanation for the former could be related to the symmetric stretching vibration of the $[CoO_2]^{3-}$ unit in an excited state. For K_3NiO_2 (d^9, Ni^+) and for K_2NiO_2 (d^8, Ni^{2+}) similar lower energy modes were deduced from the progression of the fine structure of the $^2\Delta_g$ and $^3\pi_g(P)$ excited states (absorbance spectra) 535 and 625 cm^{-1}, respectively.[6,8] Furthermore, it is worth mentioning that for K_2NiO_2 only the feature at 732 cm^{-1} (laser excitation energy 514.5 nm) is reported and assigned to the symmetric stretching vibration of the $[NiO_2]^{2-}$ complex.[8] This is in line with our results for the $[MO_2]^{3-}$ series and consistent with the change in the oxidation state from (+2) to (+1) resulting in a bathochromic shift.

4. CONCLUSIONS

We have synthesized a series of isotypic oxo-compounds containing the complex unit, $[MO_2]^{3-}$, with the transition metals M = Co, Ni, and Cu in the less-common low oxidation state (+1). These complexes can be described as coordinatively unsaturated and thus far have only been observed in the solid state. Five of six expected Raman active modes for $Na_5[NiO_2][S]$ are observed experimentally and assigned to the specific lattice eigenmodes based on their polarization properties and the results of first principle lattice dynamics calculations. We further provide a comparison of lattice modes for the members of the $Na_5[MO_2][CO_3]$ series that contain the statistically disordered carbonate ion. Assignments of the fundamental modes of the carbonate are discussed in relation to the structural aspects regarding the distortion of the cube-octahedral cavity. Ligand field calculations have been employed to account for differences in interatomic distances of the $[MO_2]^{3-}$ complexes in accordance with their respective electronic structure. The assignment of fundamental vibrational modes, ν_s and ν_{as}, of the $[MO_2]^{3-}$ complex for this series are found to be in good agreement with structural aspects. The results of our DFT calculations certainly resolve the controversial assignment in the literature based on powder data (KBr technique) collected in the mid-infrared as well as proposed by earlier theoretical work.

The calculated energies of the electronic states in the present ligand field (AOM) for the isolated $[MO_2]^{3-}$ complexes are in line with the absorbance spectra for (**1**) and (**2**).[6,27] We show that the magnetic members with d^8 and d^9 electronic configuration exhibit additional spectroscopic features (elec-

dx.doi.org/10.1021/ic300348b | *Inorg. Chem.* 2012, 51, 5822−5830

tronic Raman scattering and luminescence), that are directly related to the spin−orbit coupling of Co^{+} and Ni^{+} in a 2-fold coordination. Those features are absent, however, for the Cu-base compounds, which find its explanations in the non-magnetic d^{10} electronic configuration present. The charge transfer energy band in (**3**) appears in the blue/UV region of the electromagnetic spectrum (≈ 2.5 eV), at higher energies than the applied laser wavelength. However, the very intense red color of (**1**, **2**, **4**) does not originate from the d-d transitions and suggests that the charge transfer related band gap is shifted to lower energies for d^{8} and d^{9} configurations, for example, around 2.0 eV.

AUTHOR INFORMATION

Corresponding Author

*E-mail: amoeller@uh.edu.

Notes

The authors declare no competing financial interest.

ACKNOWLEDGMENTS

This work has been generously supported by the Welch Foundation (Grant G099857), the State of Texas through the Texas Center for Superconductivity, and the University of Houston. D.E.G. acknowledges Drs. Joan and Herman Suit for the Eby Nell McElrath fellowship. We also thank Dr. Lee M. Daniels from Rigaku Americas Corporation for valuable assistance in determining the orientation of the samples.

REFERENCES

(1) Greenwood, N. N.; Earnshaw, A. *Chemie der Elemente*; VCH: Weinheim, Germany, 1988.

(2) Losert, W.; Hoppe, R. *Z. Anorg. Allg. Chem.* **1985**, *521*, 69−78.

(3) Bernhardt, F.; Hoppe, R. *Z. Anorg. Allg. Chem.* **1993**, *619*, 969−975.

(4) Burow, W.; Birx, J.; Bernhardt, F.; Hoppe, R. *Z. Anorg. Allg. Chem.* **1993**, *619*, 923−933.

(5) Amann, P.; Möller, A. *Z. Anorg. Allg. Chem.* **2003**, *629*, 1643−1650.

(6) Möller, A.; Hitchman, M. A.; Krausz, E.; Hoppe, R. *Inorg. Chem.* **1995**, *34*, 2684−2691.

(7) Möller, A. *Z. Anorg. Allg. Chem.* **2001**, *627*, 2625−2629.

(8) Hitchman, M. A.; Stratemeier, H.; Hoppe, R. *Inorg. Chem.* **1988**, *27*, 2506−2510.

(9) (a) Schäffer, C. E.; Jørgensen, C. K. *Mol. Phys.* **1965**, *9*, 401−412. (b) Richardson, D. E. *J. Chem. Educ.* **1993**, *70*, 372−380.

(10) Möller, A. *Z. Anorg. Allg. Chem.* **2005**, *631*, 2285−2296.

(11) Perdew, J. P.; Wang, Y. *Phys. Rev. B* **1992**, *45*, 13244−13249.

(12) Delley, B. *J. Phys. Chem.* **1996**, *100*, 6107−6110.

(13) Delley, B. *J. Chem. Phys.* **2000**, *113*, 7756−7764.

(14) Monkhorst, H. J.; Pack, J. D. *Phys. Rev. B* **1976**, *13*, 5188−5192.

(15) (a) Kruse, D. A.; Davis, J. E.; Gerloch, M.; Harding, J. H.; Mackey, D. J., McMeeking, R. F. *CAMMAG, a FORTRAN computing package*; University Chemical Laboratory: Cambridge, England, 1979. (b) Riley, M. *CAMMAG for PC*, version 4.0; Univ. of Queensland: St. Lucia, Australia, 1997.

(16) Nakamoto, K. *Infrared and Raman Spectra of Inorganic and Coordination Compounds*, 6th ed.; Wiley-Interscience, John Wiley & Sons, Inc.: New York, 2009.

(17) Ehrhardt, H.; Schweer, H.; Seidel, H. *Z. Anorg. Allg. Chem.* **1980**, *462*, 185−198.

(18) Weidlein, J.; Müller, U.; Dehnicke, K. *Schwingungsspektroskopie*, 2. Auflage; Georg-Thieme Verlag: Stuttgart, Germany, 1988.

(19) Correlation tables used as given in Rousseau, D. L.; Bauman, R. P.; Porto, S. P. S *J. Raman Spectrosc.* **1981**, *10*, 253−290.

(20) Ali, N. Z.; Nuss, J.; Jansen, M. *Z. Anorg. Allg. Chem.* **2011**, *637*, 183−185.

(21) Meeks, H.; Rasing, Th.; Wyder, P.; Janner, A.; Janssen, T. *Phys. Rev. B* **1986**, *34*, 4240−4254.

(22) Brooker, M. H.; Bates, J. B. *J. Chem. Phys.* **1971**, *54*, 4788−4796.

(23) Brooker, M. H.; Bates, J. B. *Spectrochim. Acta, Part A* **1974**, *30*, 2211−2220.

(24) Scheetz, B. E.; White, W. B. *Am. Mineral.* **1977**, *62*, 36−50.

(25) Bridgeman, A. J. *J. Chem. Soc., Dalton Trans.* **1996**, *24*, 4555−4562.

(26) (a) Heyen, E. T.; Wegerer, R.; Cardona, M. *Phys. Rev. Lett.* **1991**, *67*, 144−147. (b) Cottam, G.; Lockwood, D. J. *Light scattering in magnetic solids*; John Wiley & Sons: New York, 1986.

(27) Fastje, O. Ph.D. Thesis, Universität zu Köln, Köln, Germany, 2009.